CRYSTAL GROWTH & DESIGN
2009
VOL. 9, NO. 8
3470–3476

Structure−Function Relationship of Calcium Alginate Hydrogels: A Novel Crystal-Forming Engineering

Xinping Li,[†] Qiang Shen,*[,†] Yunlan Su,[‡] Fang Tian,[†] Ying Zhao,[‡] and Dujin Wang[‡]

Key Laboratory for Colloid and Interface Chemistry of Education Ministry, School of Chemistry & Chemical Engineering, Shandong University, Ji'nan 250100, China, and Beijing National Laboratory for Molecular Sciences, Key Laboratory of Engineering Plastics, Joint Laboratory for Polymer Science and Materials, Institute of Chemistry, Chinese Academy of Sciences, Beijing 100080, China

Received February 10, 2009; Revised Manuscript Received April 13, 2009

ABSTRACT: Hydrogels of calcium alginate are the cross-linked networks containing a large fraction of water, which were used as the precursors of calcium carbonate ($CaCO_3$) mineralization for the first time. The well-defined geometry, the permeability, and the ion-exchange property of these pregels favored the facile fabrication of calcite superstructures through the slow inpouring of ammonia and carbon dioxide gases. When calcium alginate hydrogels sponged up a relatively high amount of liquid, the resulting products with the outside calcite sequences transcribed the spongelike pregel beads with the outside nucleation sites of carboxyl groups. The inner characteristic of these $CaCO_3$ superstructures showed the endocentric growth trends of calcite, indicating the permeability of hydrogel beads and the diffusing directions of permeated gases. In the presence of low liquid content, the pregels favored the formation of calcite superstructures with relatively smooth surfaces, demonstrating the inside lamellar array of calcite nanoparticles. This strategic approach indicated to a great extent the biologically controlled mineralization mechanism, dealing with (1) the preadsorption of calcium ions by the functional groups of biomolecules, (2) the confined crystallization within the three-dimensional networks, and (3) the proper arrangement of nanosized calcites by association with the organic architectures. Surprisingly, even the apparently "single-crystalline" $CaCO_3$ was proven to comprise tiny calcite rhombohedrons. Furthermore, these building blocks coaligned each other with respect to the polymers' conjugated backbones. Therefore, these suggest a novel pathway of multivalent metal pregelation phases for the biomimetic fabrication of functional materials.

1. Introduction

Sodium alginate is a hydrophilic polysaccharide that is produced by algae and bacteria. Chemically, it is a linear copolymer of two monomers, β-D-mannuronic acid (M) and α-L-guluronic acid (G) residues, joined by glycosidic links β-1, 4 and α-1, 4. In the polymer backbones, the M residue has ^{4}C1 conformation, whereas the G residue unit has ^{1}C4 conformation, regardless of the monomer number ratio (M/G) and the residue-segmented lengths.[1] Because of their natural origin and biocompatibility, alginate macromolecules are widely used in food and pharmaceutical industries.[2,3] For example, it can be used as an encapsulation material for immobilizing cells, enzymes and proteins as well as for controlled release of drugs.[4] Similarly, the gelatinization, the strength, and the porosity of the consequently formed gels caused alginates to be widely used as a construction material for membrane filtration.[5] These applications can be simply ascribed to the electrostatic force between the carboxyl groups of alginates and the counterion species (e.g., Ca^{2+}, Zn^{2+}, Cu^{2+}),[2−7] depending mainly upon the M/G ratio in polymer chains, the properties of counterions and/or additives, and the acidity of medium.[8]

Similarly, alginate molecules could also be used as crystal modifiers for material synthesis purposes. The ionic gelation by mixing zinc nitrate and sodium alginate solutions favored the preparation of nanosized ZnO particles through the thermal decomposition of zinc alginate gels, whereas the revised sol−gel technique benefited the fabrication of alkaline earth phosphates.[9] Reverse to the typically gelled process of calcium alginate,[10] calcium alginate hydrogel does not seem to be suitable for the substantive precipitation of $CaCO_3$, because that $CaCO_3$ particles are usually used as sacrificial templates for the polyelectrolyte encapsulation through a layer-by-layer pathway.[11]

Calcium carbonate is one of the most common biological materials found mainly in mollusc shells, and it has three anhydrous polymorphs of calcite, aragonite, and vaterite in calcareous structures of organisms.[12] Lots of organic compounds and their self-assemblies have been used to synthesize $CaCO_3$ crystals and control their morphologies, polymorphs, and metastable phases.[13] Up to now, there has been no report on the achievement of biological $CaCO_3$ performance design through the biomimetic approaches. In our previous works,[14] the functionalized surfactant of calcium dodecyl sulfate was used both as an organic additive and as the source of calcium ions in the precipitation process of $CaCO_3$. Although this induced the fabrication of vaterite and consequently controlled the novel phase transformation of unstable vaterite to the metastable aragonite under mild circumstances; however, the synthesized $CaCO_3$ did not simultaneously match the unique orientation, the confined crystallization, and the coalignment with the organic matrices.

Water-soluble macromolecules extracted from the biogenic calcite prisms, which are rich in the residues of aspartic and glutamic acids, could be organized into complex gels through inter- and intramolecular interactions in biological systems. Interestingly, this structural property associates well with the calcitic microstructures, probably playing a crucial role in the formation of seashells with layered structures.[15,16] In the presence of sodium alginate, the direct mixing of calcium and carbonate ions could result in the rosette-like aggregates of calcite.[17a] When sodium alginate was used for the prior treatment of porcine and human heart valves, the crystallization rate of vaterite on the surfaces of atherosclerotic aorta could be effectively inhibited.[17b] However, the use of calcium alginate hydrogels as the precursors of $CaCO_3$ mineralization is so far limited. In this paper, the structure−function relationship of

* Corresponding author. Fax: 86-531-88564750. E-mail: qshen@sdu.edu.cn.
[†] Shandong University.
[‡] Chinese Academy of Sciences.

10.1021/cg900154v CCC: $40.75
Published on Web 05/19/2009

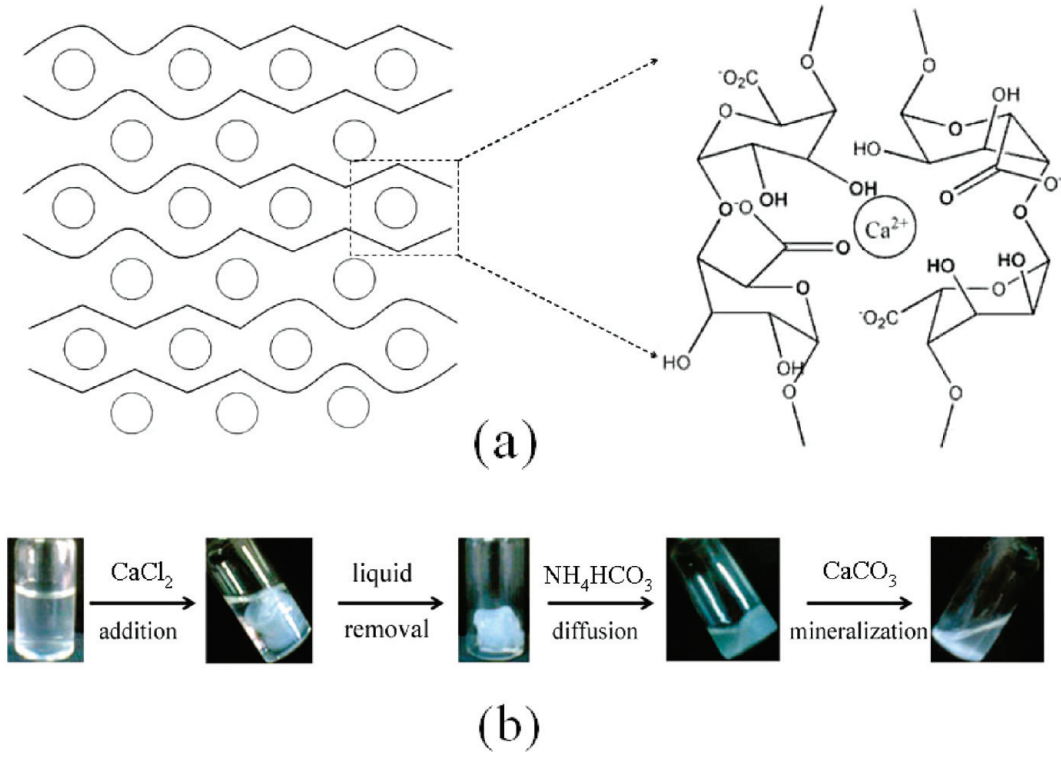

Figure 1. (a) Schematic illustration of the two-dimensional network structure of calcium alginate hydrogels. (b) Photographs of the experimental procedure adopted for the formation of calcite superstructures.

calcium alginate pregels was mainly assessed for the biomimetic fabrication of calcite superstructures.

2. Experimental Section

2.1. Materials and Hydrogel Preparation. Calcium chloride and ammonium bicarbonate are of A. R. grade. Sodium alginate powder was purchased from Sinopharm Chemical Reagent Co. Ltd. (Shanghai, China) and was used without further purification. Deionized water was used throughout the sample preparations.

The hydrogels of calcium alginate were prepared as follows. First, the aqueous solutions of sodium alginate (1.0 wt %) and calcium chloride (1.0 mol/L) were prepared. Second, a certain volume of $CaCl_2$ solution (0.5−2.0 mL) was transferred into a 10 mL glass vial containing 5 mL of sodium alginate solution. The admixture was then left undisturbed for 9 h to avoid the interfusion of air bubbles into the forming spongelike gel and to ensure the complete exchange of Ca^{2+} and Na^+ ions. Third, after the removal of excess liquid, the lumpish gel was rinsed three times using deionized water and occasionally shaking. Finally, the gel was weighed to evaluate the weight percentage of gel to the gross weight of sodium alginate and calcium chloride solutions (referred to as the percentage of sponged liquid), which was then sealed in the glass bottle waiting for the next conduct.

2.2. $CaCO_3$ Synthesis. For comparison purposes, the pregels with different weight percentage of sponged liquid were simultaneously set up under the same experimental conditions of calcium carbonate crystallization. Typically, five 10-mL vials containing a certain amount of calcium alginate hydrogels and a dish (diameter ≈ 63 mm, depth ≈ 12 mm) containing 2.0 g ammonium bicarbonate were placed in a closed chamber (∼ 800 mL) at 30 °C. The dish and the five glass bottles were sealed with parafilm, and the covered films were punched with 3 needle-holes for the diffusion of ammonia (NH_3) and carbon dioxide (CO_2) gases. The slow diffusion and the subsequent dissolution of NH_3 and CO_2 gases into the gelatin phase then caused the breakage of the cross-linked structures and the simultaneous crystallization of $CaCO_3$. Unless otherwise stated, the chamber was kept under the thermostatic condition for 15 days. Finally, after the removal of the clear supernatant, the resulting precipitates were removed from solution, rinsed three times with deionized water followed by three rinses with ethanol, and then dried at room temperature for 1 day.

2.3. Crystal Characterization. The collected solids were Au-coated prior to examination by a JEOL JSM-7600F scanning electron microscope (SEM), fitted with a field-emission source and operating at an accelerating voltage of 15 kV. The X-ray diffraction (XRD) patterns were performed on a Rigaku D/max-2400 powder X-ray diffractometer with Cu Kα radiation (40 kV, 120 mA). The 0.02 ° steps/(25 s) and the 2θ range from 20 to 60° were selected to analyze the crystal structure and orientation. TGA measurements were carried out on a Mettler to monitor the weight loss of $CaCO_3$ at a heating rate of 10 °C/min from room temperature to 850 °C under a nitrogen atmosphere. The Fourier transform infrared spectroscopy (FT IR) measurements were performed on a VERTEX-70 spectrometer using KBr tablet method, with a scanning region of 4000−400 cm^{-1} and resolution of 4 cm^{-1}. For the time-dependent experiments, the $CaCO_3$ crystallization reactions were stopped and the systems were lyophilized to obtain the cottonlike composites of ammonium alginate and $CaCO_3$, which were used directly for the corresponding SEM observation and the FT IR characterization.

3. Results and Discussion

3.1. Effect of Gel Structural Properties. Generally, the commercial sodium alginate has a broad molecular weight distribution and undefined M/G ratio, and the polymer structure varies widely, depending upon the survival environments of algae and bacteria. Nevertheless, when dispersed in deionized water, sodium alginate is always negatively charged at neutral pH because of the dissociation of carboxyl groups (i.e., $-COO^-$). These $-COO^-$ groups are specific to calcium ionic binding, and the relative theories have deduced that the addition of calcium ions into the aqueous solution of sodium alginate promotes the chain dimerization of polyelectrolytes, especially for the pairing of G residues.[18] Therefore, calcium alginate hydrogels are the cross-linked networks sponged up a large quantity of liquid, which can be schematically illustrated in Figure 1a.

As shown in Figure 1a, the $-COO^-$ sequences on an alginate backbone configuration resemble the N-terminal parts of an

unfolded polypeptide. Interestingly, the polypeptide backbones of mollusc shell proteins possess anionic and cationic electrostatic "pocket" regions on the surfaces, which are responsible for the adsorption of calcium ions and for the consequent calcite hillock overgrowth.[16a,19] On the basis of the unique conformation and the multifunctional features of nacre-associated proteins, the well-defined geometry, the permeability, and the ion-exchange properties of calcium alginate gels could be expected for the mineralization of $CaCO_3$. The experimental procedure adopted for the biomimetic fabrication of $CaCO_3$ was recorded, shown in Figure 1b. This could be described with the following steps: the gelation of sodium alginate, the removal of excess liquids, the diffusion of NH_3 and CO_2 gases, the gel-to-sol transformation and the simultaneous precipitation of $CaCO_3$.

After the direct mixing of sodium alginate and calcium chloride solutions, the concentration of calcium ions and the pH value of the admixing system did not exert a great influence on the microstructure of calcium alginate gels; nevertheless, the amount and nature of sponged liquid substantially affected the porosity and mechanical strength of gel networks.[3a] Additionally, as illustrated in Figure 1b, the mineralization of $CaCO_3$ corresponds with the simultaneous gel−sol transformation, indicating the meaningless of the mechanical strength. Therefore, the amount and the acidity of sponged liquid in the pregels were considered to assay the mineralization of $CaCO_3$. It should be emphasized that all the precipitates sampled from these pregels were proven to be the thermodynamically stable calcite containing 2.3 ± 0.6 wt % polysaccharide (see Figure S1 in the Supporting Information).

When the gelled phases sponged up 71.1 wt % liquid, the resulting calcite displayed mainly the spherical superstructures with the densely covered steps of rhombohedrons (Figure 2a). Also, there were the apparently "single-crystalline" particles of calcite marked with white arrows, because of the crystallization of $CaCO_3$ in relatively big water domains. The cross-section of a spherical $CaCO_3$ showed the radiation pattern from the center (Figure 2b), suggesting that the diffusion of CO_2 gas into the center of spherical pregel beads promoted the depletion of calcium ions and the simultaneous crystal growth of calcite. When the sponged percentage of liquid decreased to 47.8 wt %, the hollow superstructures of calcite marked with the black arrows were observed (Figure 2c). If there were big interspaces in pregel networks, the leaching of the encapsulated liquid could cause the formation of hollow structures.

When the sponged amount of liquid in gel precursors further decreased, the resulting calcite spheres displayed the surfaces decorated with the relatively small rhombohedrons (see Figure S2 in the Supporting Information). The morphological evolution of representative calcite spheres with the sponged amount of liquid was shown in Figure 3. As shown in Figure 2, the calcite superstructures obtained at an high amount of sponged liquid possessed staircase-like blocks with the exposed [104] crystalline faces (Figure 3a) and radiation pattern for the inner characteristic (Figure 3b). The decreasing amount of sponged liquid means the increasing density of $-COO^-$ groups on a gel bead surface; which caused the dimensions of surface-localized calcite blocks to decrease, resulting in $CaCO_3$ superstructures with the terracelike surfaces (Figure 3c). Occasionally, the irregular water channels perpendicular to the pathway of CO_2 diffusion could possibly cause the formation of valleys in a calcite superstructure (Figure 3d). Finally, the presence of low amount of sponged liquid resulted in cobblestone-like superstructures with subtile calcite blocks on the surfaces (Figure 3e, f). Indeed, the magnified picture of the cross-section of a cobblestone showed

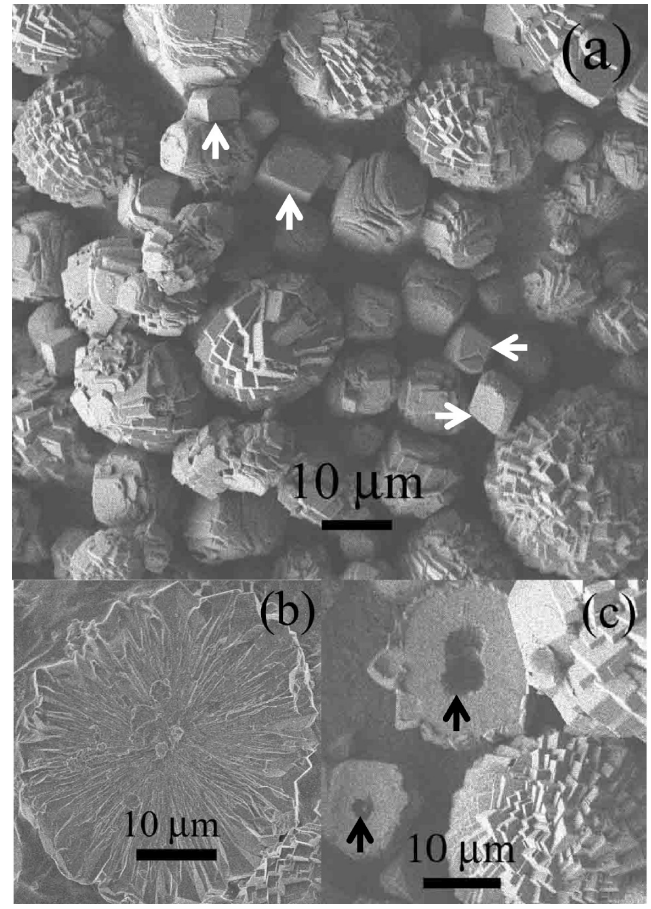

Figure 2. SEM images of calcite superstructures obtained from the calcium alginate hydrogels sponged up (a, b) 71.1 and (c) 47.8 wt % liquid, respectively. The $CaCO_3$ marked with white arrows were the visually determined "single-crystal" particles of calcite, and these marked with black arrows were the hollow calcite superstructures.

partly the lamellar array of calcite building blocks (see Figure S3 in the Supporting Information), coinciding with the two-dimensional network structure of calcium alginate hydrogels shown in Figure 1a.

When sodium alginate solution (1.0 wt %) was adjusted to pH 4.0 or 10.5 by the addition of HCl (1.0 mol/L) or NaOH solution (1.0 mol/L), herein the pregels obtained by the consequent addition of calcium chloride were referred to as the acidic/alkaline gels of calcium alginate. In comparison with the neutral pregels' results shown in Figure 3, the acidic and alkaline pregels exerted similar swelling-effectiveness on the morphological evolution of calcite superstructures (data omitted). The same experimental results were also obtained by adjusting the acidity of the neutral pregel in the presence of 10.0 mmol/L aspartic acid (see Figure S4 in the Supporting Information).

Because the pK_a values of G and M monomers range from 3 to 4, the previous protonation/deprotonation of alginate molecules should alter the hydrophilic property of polymer backbones and the possible chain dimerization mechanisms in the aqueous media.[20] The calcium alginate hydrogels obtained at different pH could sponge different amount of liquid (see Figure S5-a in the Supporting Information). For example, when the pregelled networks were constructed by the addition of $CaCl_2$ solution (1.0 mol/L, 0.1 mL) into the aqueous systems of sodium alginate (1.0 wt %, 5.0 mL), the percentage of sponged liquids were 60.6, 71.1, and 96.0 wt % at pH values of 4.5, 7.0, and 10.5, respectively. At different pH levels, the apparently same

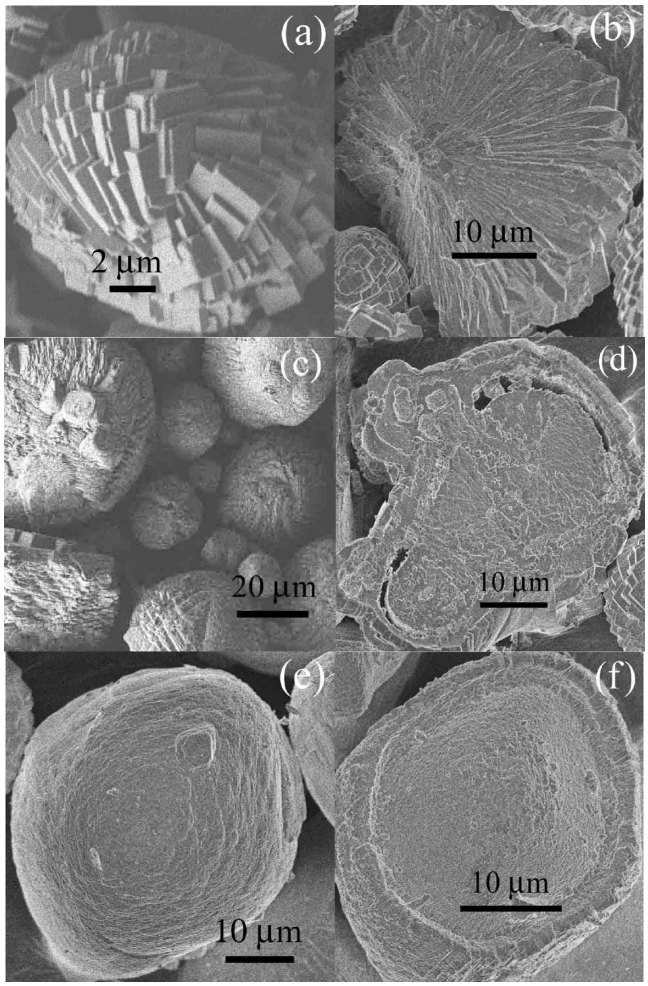

Figure 3. SEM images of calcite superstructures and the corresponding cross sections obtained from the calcium alginate hydrogels sponged up (a, b) 71.1, (c, d) 37.5, and (e, f) 27.6 wt % liquid, respectively.

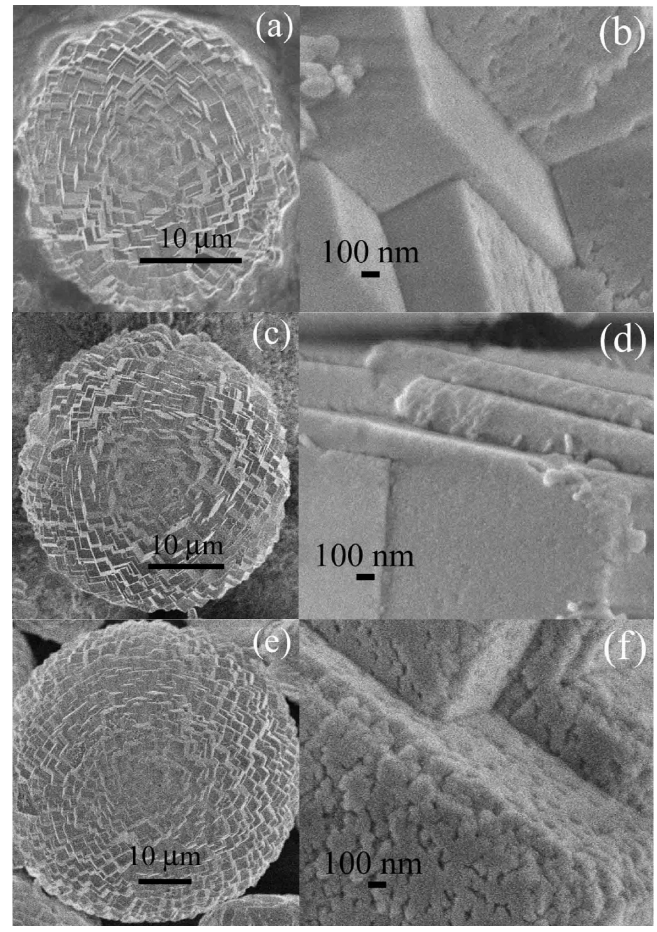

Figure 4. SEM images of calcite superstructures obtained from the calcium alginate hydrogels at the pH values of (a, b) 7.0, (c, d) 4.0, and (e, f) 10.5, respectively. Panels b, d, and f are the magnified pictures of panels a, c, and e, respectively.

calcite superstructures were shown in panels a, c, and e of Figure 4, respectively. Interestingly, when these surface-localized blocks were magnified, the morphological discrepancy could be observed, shown in panels b, d, and f of Figure 4, respectively. These might be due to the different gelation mechanisms of calcium alginate at different pH (see Figure S5-b in the Supporting Information).[18,20]

3.2. Crystal-Forming Engineering. From the viewpoints of biomineralization, the biologically controlled process comprises of several coherent steps: extraction and enrichment of calcium and carbonate ions, nucleation, and confined crystallization of $CaCO_3$, arrangement and crystallographic orientation of crystallites. If the pregels of calcium alginate, together with the slowly inpouring of CO_2 gas, can be used to simulate the extraction and enrichment of calcium and carbonate ions onto biomolecule surfaces,[16,21] the following $CaCO_3$ mineralization results should correlate, to a great extent, with the in vivo biologically controlling steps.

During the time-dependent experiments of $CaCO_3$ mineralization, the reactions were stopped and the systems were lyophilized to track the formation process of calcite superstructures (Figure 5 and Figure S6 in the Supporting Information). The lyophilized pregels exhibited the cracked sheet-like structure (Figure 5a and Figure S6-a in the Supporting Information), which was due to the lamellar arrangement of cross-linked alginate molecules with the high swelling degree. Figure 5b, as well as Figure S6-b in the Supporting Information, further indicated that these sheets comprised the gel spheres of calcium alginate.[10b] As the continuous inpouring of CO_2 and NH_3 gases progressed, no substantial difference was observed in the appearance of the gel sheets, except for the increasing emergence of macro-concaves. This could be seen from panel c to e then g of Figure 5. Correspondingly, the $CaCO_3$ crystallites (i.e., the rhombohedral particles) could be observed to localize the surfaces of gel beads at the reaction time of 4 h (Figure 5d, panels c and d of Figure S6 in the Supporting Information). With the proceeding of $CaCO_3$ mineralization, the gel−sol transformation continued and the $CaCO_3$ superstructure with the terracelike morphology (Figure 5f) and that with staircase steps on the surface (Figure 5h) were obtained consequently.

FT IR characterization of these lyophilized samples was also conducted to follow the mineralization process of $CaCO_3$ (Figure 6). The variations of infrared absorption peaks and the appearance of new absorption bands were observed as a function of reaction time, however, only the major were described herein. From the curves a and b in Figure 6, the broad absorption peaks at 1627 and 1437 cm^{-1} could be assigned to the asymmetric and the symmetric stretching vibration of $-COO^-$ groups, respectively.[22] As the reaction time proceeded, the mineralization of $CaCO_3$ could be confirmed by the appearance of asymmetric stretching (1411 cm^{-1}), out-of-plane deformation

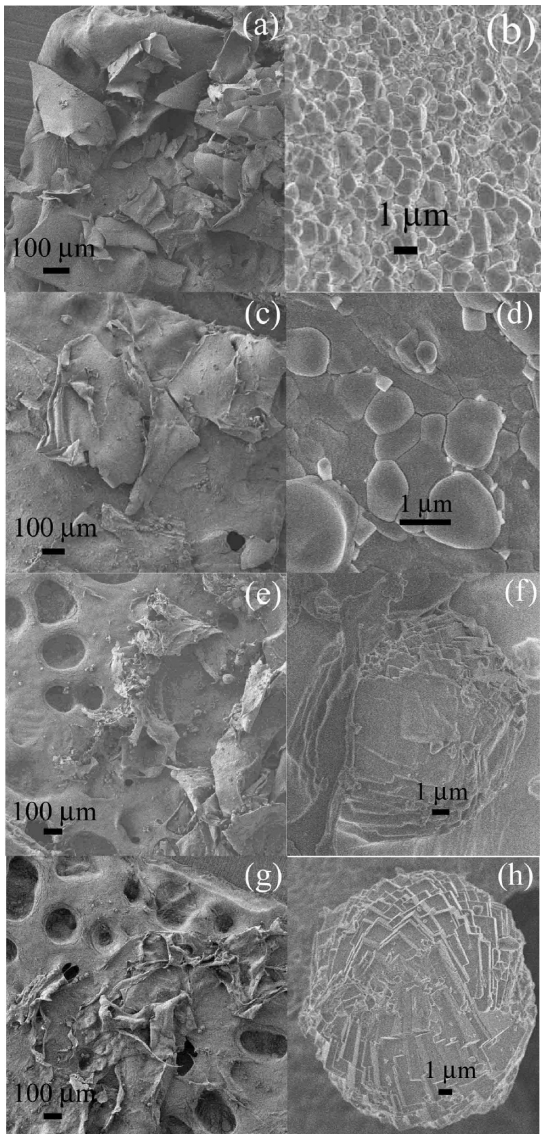

Figure 5. SEM images of the lyophilized hydrogels of calcium alginate sampled at the reaction intervals of (a, b) 0, (c, d) 4, (e, f) 8, and (g, h) 12 h, respectively. Panels b, d, f, and h are the magnified pictures of panels a, c, e, and g, respectively.

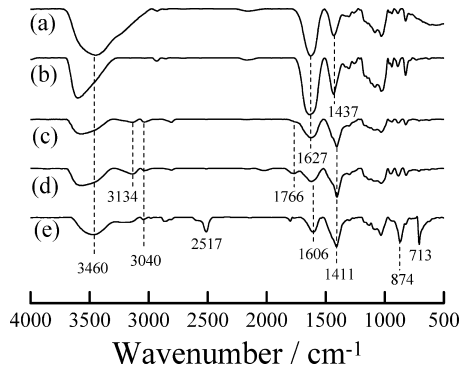

Figure 6. FT IR spectra of sodium alginate powder (a) and the lyophilized hydrogels of calcium alginate at the reaction intervals of (b) 0, (c) 4, (d) 8, and (e) 12 h, respectively.

(874 cm^{-1}), and in-plane deformation (713 cm^{-1}) characteristics of calcite, [23,24] shown in Figure 6c−e.

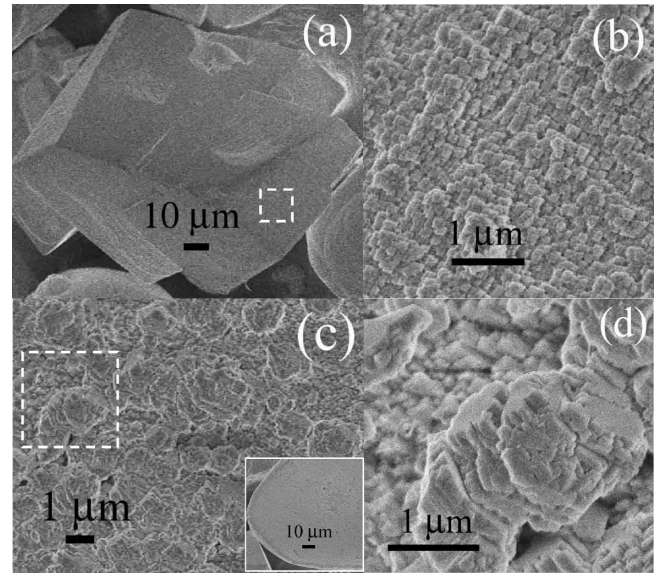

Figure 7. SEM images of calcite superstructures obtained from the calcium alginate hydrogels sponged up 27.6 wt % liquid. The marked squares in panels a and c were magnified, shown in panels b and d, respectively. The inset is the low-resolution SEM image of panel c.

Generally, calcite precipitated in the presence of biopolymers exhibited the asymmetric stretching vibration peaked at ∼1420 cm^{-1}.[17c,24] Despite the overlapping between the asymmetric stretch of carbonates and the symmetric stretching vibration of alginate $-COO^-$ groups, the peak position of the latter with a shift to lower wavenumber, together with its relative peak intensity compared with that of $-COO^-$ asymmetric stretching absorption, clearly proved the replacement of calcium ions on the alginate backbones.[22a] Although the irregular variations (i.e., the shape and the shift) of O−H absorption band (∼3460 cm^{-1}) and its shoulder (∼3134 cm^{-1}) were unexplained, the lowering of ∼3460 cm^{-1} band intensity was indicative of a decrease in alginate intramolecular bonding because of the gradual consumption of calcium ions.[22] In parallel, the appearance of the stretching vibrations for the N−H (∼3040 cm^{-1}) and the C═O (1766 cm^{-1}) bonds of amide groups, as well as the observation of CO_2 adsorption peak at 2517 cm^{-1},[22c,24a] further demonstrated the gel-sol transformation of calcium alginates to the ammonium salts.

Surprisingly, in the presence of 27.6 wt % sponged liquid, lots of the apparently "single-crystalline" particles of calcite were observed (Figure 7a). When part of the pseudorhombohedral particle was magnified (Figure 7b), it displayed the lamellar array of well-proportioned calcite rhombohedrons. This implies that nanocrystalline calcite blocks were lamellar stacked to match the polymer-controlled crystal growth,[25] or the alginate molecules were homogeneously embedded in the oriented architecture of calcite. Similarly, when a superstructure section was magnified (Figure 7c and the corresponding inset), the lamellar array of asymmetric calcites was also observed (Figure 7d). If the cross-linking knots in pregel networks acted as the nucleation sites of calcite, these could demonstrate the in situ confined crystallization and the consequently oriented aggregation of inorganic building blocks via the interactions between alginate backbones. Furthermore, a comparison of images b and d in Figure 7 shows the apparent difference between the aggregation states of inorganic nanoparticles, possibly correlating with the chain dimerization of differently segmented G and M residues.

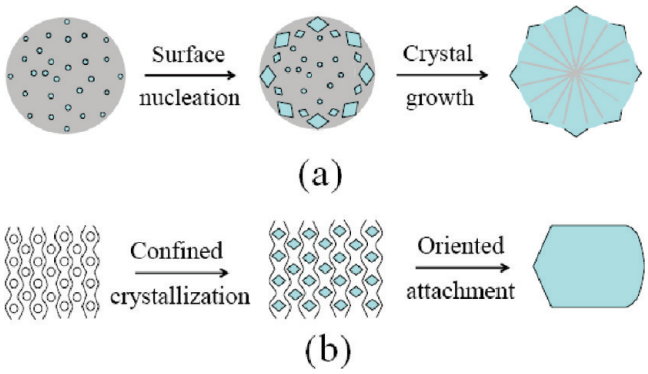

Figure 8. Two-dimensional cartoons for the structure−function relationship of calcium alginate hydrogels sponged up the relatively (a) high and (b) low amounts of liquid, respectively.

By the above listed results, the crystal-forming engineering of calcium alginate pregels could be classified by the weight percentage of sponged liquid. At the relatively high amount of sponged liquid, the universally obtained calcite superstructures, with the outside steps of rhombohedrons and the inner radiation pattern, macroscopically indicate the surface nucleation and the consequent crystal growth of calcites. Thus, the pregel bead template-mediated formation mechanism of $CaCO_3$ can be schematically illustrated in Figure 8a. It has been reported that in the processes of biomineralization and biomimetic approaches, [25] the organic−inorganic binding affinity exerted a great influence on the self-assemblies of inorganic particles, as did the fusion of oriented crystals and the complex interactions between adsorbed organics. Therefore, the $CaCO_3$ mineralization in the compact network of calcium alginate pregels could be schematically illustrated in Figure 8b. This summarizes the two crystal-forming steps: the confined crystallization of calcite and the consequent arrangement of building blocks.

4. Conclusions

In summary, the pregelation of calcium alginate and the consequently slow inpouring of CO_2 gas simulated to a great extent the extraction and enrichment of calcium and carbonate ions by invertebrate secretions. These favor the selective nucleation and the consequently confined crystallization of $CaCO_3$ within the diminishing pregel beads of calcium alginate, resulting in the spherical superstructures of calcite. Similarly, the proper arrangement of nanosized calcites in the three-dimensional networks of calcium alginate, followed by the leaching of sponged liquids and the fusing of crystalline blocks, could result in the apparently single-crystalline particles of calcite. These correlated the coalignment of calcite building blocks with the polymers' conjugated backbones. In one word, the morphologies and the inner characteristics of $CaCO_3$ products depended upon the structural properties of calcium alginate hydrogels, suggesting the structure−function relationship of multivalent metal pregelation phases for the biomimetic fabrication of functional materials.

Acknowledgment. The financial support from the National Natural Science Foundation of China (20773079 and 20833010), from the National Basic Research Program of China (2009CB930802), from the NCET Program in University, and from the Science and Technology Development Plan of Shandong Province (2007GG10003004) is gratefully acknowledged.

Supporting Information Available: XRD profile and TGA curves of $CaCO_3$ samples (Figure S1), SEM images of various calcite superstructures (Figures S2−S4), the sponged amount curves and FT IR spectra of calcium alginate pregels (Figure S5), and the transmission optical photographs of lyophilized samples (Figure S6) (PDF). This material is available free of charge via the Internet at http://pubs.acs.org.

References

(1) (a) Klöck, G.; Pfeffermann, A.; Ryser, C.; Gröhn, P.; Kuttler, B.; Hahn, H.-J.; Zimmermann, U. *Biomaterials* **1997**, *18*, 707–713. (b) Salomonsen, T.; Jensen, H. M.; Stenbæk, D.; Engelsen, S. B. *Carbohydr. Polym.* **2008**, *72*, 730–739.

(2) (a) Roopa, B. S.; Bhattacharya, S. *J. Food Eng.* **2008**, *85*, 123–131. (b) Montero, P.; Pérez-Mateos, M. *Food Hydrocolloids* **2002**, *16*, 375–385.

(3) (a) Sriamornsak, P.; Kennedy, R. A *Int. J. Pharm.* **2006**, *323*, 72–80. (b) Broderick, E.; Lyons, H.; Pembroke, T.; Byrne, H.; Murray, B.; Hall, M. *J. Colloid Interface Sci.* **2006**, *298*, 154–161.

(4) (a) Yu, C.-Y.; Jia, L.-H.; Yin, B.-C.; Zhang, X.-Z.; Cheng, S.-X.; Zhuo, R.-X. *J. Phys. Chem. C* **2008**, *112*, 16774–16778. (b) Gill, I. *Chem. Mater.* **2001**, *13*, 3404–3421.

(5) (a) Mammarella, E. J.; Rubiolo, A. C. *Chem. Eng. J.* **2003**, *94*, 73–77. (b) Pileva, F. M.; Mattiasson, B. *Ind. Eng. Chem. Res.* **2008**, *47*, 4131–4141.

(6) (a) Zhang, H.; Tumarkin, E.; Peerani, R.; Nie, Z.; Sullan, R. M. A.; Walker, G. C.; Kumacheva, E. *J. Am. Chem. Soc.* **2006**, *128*, 12205–12210. (b) Perullini, M.; Jobbágy, M.; Moretti, B. M.; García, S. C.; Bilmes, S. A. *Chem. Mater.* **2008**, *20*, 3015–3021.

(7) (a) Gardea-Torresdey, J. L.; Becker-Hapak, M. K.; Hosea, J. M.; Darnall, D. W. *Environ. Sci. Technol.* **1990**, *24*, 1372–1378. (b) Davis, T. A.; Kalis, E. J. J.; Pinheiro, J. P.; Town, R. M.; van Leeuwen, H. P. *Environ. Sci. Technol.* **2008**, *42*, 7242–7247.

(8) (a) Braccini, I.; Pérez, S. *Biomacromolecules* **2001**, *2*, 1089–1096. (b) Draget, K. I.; Strand, B.; Hartmann, M.; Valla, S.; Smidsrød, O.; Skjåk-Bræk, G. *Int. J. Biol. Macromol.* **2000**, *27*, 117–122. (c) Puttipipatkhachorn, S.; Pongjanyakul, T.; Priprem, A. *Int. J. Pharm.* **2005**, *293*, 51–62.

(9) (a) Baskoutas, S.; Giabouranis, P.; Yannopoulos, S. N.; Dracopoulos, V.; Toth, L.; Chrissanthopoulos, A.; Bouropoulos, N. *Thin Solid Films* **2007**, *515*, 8461–8464. (b) Sugiyama, S.; Fuji, M.; Fukuta, K.; Seyama, K.; Sotowa, K.-I.; Shigemoto, N. *J. Colloid Interface Sci.* **2006**, *295*, 141–147.

(10) (a) Chai, Y.; Mei, L.-H.; Lin, D.-Q.; Yao, S.-J. *J. Chem. Eng. Data* **2004**, *49*, 475–478. (b) Robitzer, M.; David, L.; Rochas, C.; Renzo, F. D.; Quignard, F. *Langmuir* **2008**, *24*, 12547–12552.

(11) (a) Zhao, Y.; Carvajal, M. T.; Won, Y.-Y.; Harris, M. T. *Langmuir* **2007**, *23*, 12489–12496. (b) Stein, E. W.; Volodkin, D. V.; McShane, M. J.; Sukhorukov, G. B. *Biomacromolecules* **2006**, *7*, 710–719. (c) Volodkin, D. V.; Larionova, N. I.; Sukhorukov, G. B. *Biomacromolecules* **2004**, *5*, 1962–1972.

(12) (a) Mann, S. *Biomineralization−Principles and Concepts in Bioinorganic Materials Chemistry*; Compton, R. G., Davies, S. G., Evans, J., Eds.; Oxford University Press: Oxford, U.K., 2001; pp 6−10. (b) Watanabe, N. In *Progress in Crystal Growth and Characterization*; Pamplin, B. R., Ed.; Pergamon Press: New York, 1981; Vol. 4, pp 99−147.

(13) (a) Meldrum, F. C. *Int. Mater. Rev.* **2003**, *48*, 187–224. (b) Demadis, K. D.; Katarachia, S. D. *Phosphorus, Sulfur, Silicon* **2004**, *179*, 627–648. (c) Buijnsters, P. J. J. A.; Donners, J. J. J. M.; Hill, S. J.; Heywood, B. R.; Nolte, R. J. M.; Zwanenburg, B.; Sommerdijk, N. A. J. M. *Langmuir* **2001**, *17*, 3623–3628. (d) Donners, J. J. J. M.; Nolte, R. J. M.; Sommerdijk, N. A. J. M. *J. Am. Chem. Soc.* **2002**, *124*, 9700–9701. (e) Ajikumar, P. K.; Wong, L. G.; Subramanyam, G.; Lakshminarayanan, R.; Valiyaveettil, S. *Cryst. Growth Des.* **2005**, *5*, 1129–1139. (f) Chibowski, E.; Szczes, A.; Holysz, L. *Langmuir* **2005**, *21*, 8114–8122. (g) Hosoda, N.; Sugawara, A.; Kato, T. *Macromolecules* **2003**, *36*, 6449–6452.

(14) (a) Shen, Q.; Wang, L. C.; Huang, Y. P.; Sun, J. L.; Wang, H. H.; Zhou, Y.; Wang, D. J. *J. Phys. Chem. B* **2006**, *110*, 23148–23153. (b) Shen, Q.; Wang, L. C.; Li, X. P.; Liu, F. L. *Cryst. Growth Des.* **2008**, *8*, 3560–3565.

(15) (a) Weiner, S. *Biochemistry.* **1983**, *22*, 4139–4145. (b) Levi-Kalisman, Y.; Falini, G.; Addadi, L.; Weiner, S. *J. Struct. Biol.* **2001**, *135*, 8–

17. (c) Pokroy, B.; Zolotoyabko, E.; Adir, N. *Biomacromolecules* **2006**, *7*, 550–556.
(16) (a) Orme, C. A.; Noy, A.; Wierzbicki, A.; Mcbride, M. T.; Grantham, M.; Teng, H. H.; Dove, P. M.; DeYoreo, J. J. *Nature* **2001**, *411*, 775–779. (b) Lakshminarayanan, R.; Joseph, J. S.; Kini, R. M.; Valiyaveettil, S. *Biomacromolecules* **2005**, *6*, 741–751.
(17) (a) Butler, M. F.; Glaser, N.; Weaver, A. C.; Kirkland, M.; Heppenstall-Butler, M. *Cryst. Growth Des.* **2006**, *6*, 781–794. (b) Kanakis, J.; Malkaj, P.; Petroheilos, J.; Dalas, E. *J. Cryst. Growth* **2001**, *223*, 557–564. (c) Manoli, F.; Dalas, E. *J. Mater. Sci.* **2002**, *13*, 155–158.
(18) (a) Matricardi, P.; Pontoriero, M.; Coviello, T.; Casadei, M. A.; Alhaique, F. *Biomacromolecules* **2008**, *9*, 2014–2020. (b) Donati, I.; Benegas, J. C.; Cesàro, A.; Paolerri, S. *Biomacromolecules* **2006**, *7*, 1587–1596. (c) Grant, G. T.; Morris, E. R.; Rees, D. A.; Smith, P. J. C.; Thom, D. *FEBS Lett.* **1973**, *32*, 195–198.
(19) (a) DeYoreo, J. J.; Dove, P. M. *Science* **2004**, *306*, 1301–1302. (b) Elhadj, S.; DeYoreo, J. J.; Hoyer, J. R.; Dove, P. M. *Proc. Natl. Acad. Sci. U.S.A.* **2006**, *103*, 19237–19242. (c) Kim, I. W.; Darragh, M. R.; Orme, C.; Evans, J. S. *Cryst. Growth Des.* **2006**, *6*, 5–10. (d) Collino, S.; Evans, J. S. *Biomacromolecules* **2007**, *8*, 1686–1694.
(20) (a) Kong, H. J.; Kim, C. J.; Huebsh, N.; Weitz, D.; Mooney, D. J. *J. Am. Chem. Soc.* **2007**, *129*, 4518–4519. (b) Cao, Y.; Shen, X.; Chen, Y.; Guo, J.; Chen, Q.; Jiang, X. *Biomacromolecules* **2005**, *6*, 2189–2196. (c) Sarmento, B.; Ferreira, D.; Veiga, F.; Ribeiro, A. *Carbohydr. Polym.* **2006**, *66*, 1–7.
(21) (a) Hartgerink, J. D.; Beniash, E.; Stupp, S. I. *Science* **2001**, *294*, 1684–1688. (b) Boskey, A. L. *J. Cell Biochem.* **1998**, *30/31*, 83–91. (c) Xu, G.; Yao, N.; Aksay, I. A.; Groves, J. T. *J. Am. Chem. Soc.* **1998**, *120*, 11977–11985.
(22) (a) Sartori, C.; Finch, D. S.; Ralph, B.; Gilding, K. *Polymer* **1997**, *38*, 43–51. (b) Leal, D.; Matsuhiro, B.; Rossi, M.; Caruso, F. *Carbohydr. Res.* **2008**, *343*, 308–316. (c) Tam, S. K.; Dusseault, J.; Polizu, S.; Ménard, M.; Hallé, J.-P.; Yahia, L.-H. *Biomaterials* **2005**, *26*, 6950–6961.
(23) (a) Aizenberg, J.; Lambert, G.; Weiner, S.; Addadi, L. *J. Am. Chem. Soc.* **2002**, *124*, 32–39. (b) Shen, Q.; Wei, H.; Zhou, Y.; Huang, Y. P.; Yang, H. R.; Wang, D. J.; Xu, D. F. *J. Phys. Chem. B* **2006**, *110*, 2994–3000.
(24) (a) Berman, A.; Ahn, D. J.; Lio, A.; Salmeron, M.; Reichert, A.; Charych, D. *Science* **1995**, *269*, 515–518. (b) Manoli, F.; Koutsopoulos, S.; Dalas, E. *J. Cryst. Growth* **1997**, *182*, 116–124. (c) Manoli, F.; Dalas, E. *J. Cryst. Growth* **1999**, *204*, 369–375.
(25) (a) Li, M.; Schnablegger, H.; Mann, S. *Nature* **1999**, *402*, 393–395. (b) Yu, S.-H.; Cölfen, H. *J. Mater. Chem.* **2004**, *14*, 2124–2147. (c) Oaki, Y.; Kotachi, A.; Miura, T.; Imai, H. *Adv. Funct. Mater.* **2006**, *16*, 1633–1639.

CG900154V